CrystEngComm

COMMUNICATION

View Article Online
View Journal | View Issue

Cite this: *CrystEngComm*, 2015, **17**, 503

Received 2nd August 2014,
Accepted 4th October 2014

DOI: 10.1039/c4ce01600a

www.rsc.org/crystengcomm

Multi-functional Au/CdS/Fe_3O_4/RGO hybrid nanomaterials with enhanced photocatalytic activity†

Yunqing Luo,* Shanshan Fan, Nongyi Hao, Shuangling Zhong and Wencong Liu*

A facile and low-cost layer-by-layer technology has been developed to synthesize a multi-functional Au/CdS/Fe_3O_4/reduced graphene oxide (RGO) hybrid nanomaterial. The RGO nanosheets are indispensable, as they act not only as a supporter to hold the multiple components together, but also as an electron acceptor and transporter to efficiently hinder the recombination of the photogenerated electron–hole pairs.

Cadmium sulfide (CdS), as a typical visible light (VL)-driven semiconductor photocatalyst used to efficiently degrade the various pollutants in water, has been studied extensively because of its relatively narrow band gap (2.42 eV) compared to TiO_2 (3.2 eV), which makes CdS a competitive candidate for photocatalysts in facilitating the utilization of VL.[1–3] However, CdS has two inherent defects. First, the fast recombination of photo-generated electron–hole pairs in CdS particles makes the catalyst idle.[4] And second, CdS particles are not stable and tend to aggregate, which results in a reduced surface area and a higher recombination rate of the photoinduced electron–hole pairs.[5] To solve these problems, various investigations have been carried out to improve the efficiency of the photocatalytic activity of CdS by preparing nanocomposites containing CdS and other semiconductors, such as TiO_2,[6] ZnO,[7] MoS_2,[8] PdS (ref. 9) or layered titanate nanosheets.[10] The preparation of quantum-sized CdS and deposition of noble metals are also considered to be appropriate methods to restrain the fast recombination of electrons and holes. As described by R. M. Navarro, the enhancement in activity caused by adding a small amount of noble metals can be explained in terms of a photo-electro-chemical mechanism, in which the electrons generated by light irradiation of the semiconductor transfer to the loaded noble metal particles, while the holes remain in the semiconductors, resulting in a decrease in the electron–hole recombination.[11] Thus, it is very necessary and urgent to design a reasonable noble metal/CdS hybrid nanostructure to optimize the photocatalytic performance.

On the other hand, considering the high toxicity of Cd^{2+}, the CdS catalyst must be recovered well after the catalytic reaction in order to avoid secondary pollution. Recently, the development of graphene-based science has brought us a solution to solve the above problem. Graphene, as a new member of the carbon family, has generated increasing interest in both fundamental science and potential applications due to its good conductivity, high electron mobility, superior chemical stability and large surface-to-volume ratio.[12,13] Excellent works on graphene materials decorated with CdS nanoparticles (NPs) are springing up. For example, a reduced graphene oxide (RGO)/CdS hybrid material was synthesized by Zheng's group *via* a one-step solvothermal method.[2] As the supporting material for the CdS NPs, RGO effectively enhanced their photocatalytic activities for the photodegradation of methylene blue in aqueous solution. Liu's group has reported the successful synthesis of GO/CdS/Pt nanocomposites with different amounts of Pt NPs *via* the formic acid reduction process followed by a two-phase mixing method.[14] The increased photocatalytic hydrogen generation efficiency is attributed to the effective charge separation and decreased anti-recombination with the addition of GO and Pt, as well as the low overpotential of Pt for water splitting. A series of CdS-graphene nanocomposites with different weight addition ratios of graphene have been synthesized as VL-driven photocatalysts for the selective transformation of alcohols to the corresponding aldehydes by Xu *et al.*[15] Shen's group presented a facile approach for the preparation of graphene/CdS nanocomposites through simple reflux processes, the CdS NPs were densely and uniformly deposited on the graphene sheets.[16] The successful hybridization of CdS and graphene could be attributed the large surface area of GO and the large number of functional groups on the GO surface. Using a similar synthetic principle, a lot of works

College of Resources and Environment, Jilin Agricultural University, Changchun, 130118, PR China. E-mail: qyluo2014@163.com, chemliuwc@163.com

† Electronic supplementary information (ESI) available. See DOI: 10.1039/c4ce01600a

have been focused on the fabrication of magnetic composite/graphene hybrids: Fe_3O_4/graphene.[17–20] The magnetic response properties could make the sample achieve the goal of fast separation from both the synthetic and application systems. To the best of our knowledge, there is still no report about the successful combination of noble metal/CdS and a Fe_3O_4/graphene composite.

Taking into account the above thinking, a good catalyst should be highly active, environmentally-friendly and recyclable. So, a new type of multi-component and multi-functional hybrid nanostructure, Au/CdS/Fe_3O_4/RGO, has been designed. Herein, CdS is the photocatalytic active center and Au is used as an assistant catalyst to enhance the catalytic performance under visible radiation. More importantly, the graphene nanosheet plays the key role of co-supporter to hold both Au/CdS and Fe_3O_4 together to form the single entity.

As described in Scheme 1, Fe_3O_4/RGO was firstly prepared *via* a hydrothermal method. The aqueous solution of GO, $FeCl_2$ and $FeCl_3$ was heated to 80 °C under argon, followed by adding $NH_3{\cdot}H_2O$ to start the *in situ* co-precipitation reaction. The corresponding TEM images are shown in Fig. S1,† and 10–30 nm Fe_3O_4 NPs were loaded onto the RGO surface uniformly. No scattered nanoparticles are found outside the RGO nanosheets. Because of the presence of ammonia and the increased temperature, the GO was reduced to RGO simultaneously. Thanks to the presence of Fe_3O_4, the products could be easily and quickly separated from the reaction solution with the help of a magnet.

In the next step, to decorate CdS NPs on Fe_3O_4/RGO, $CdCl_2{\cdot}(H_2O)_{2.5}$ and thiourea ($CS(NH_2)_2$) were used as the Cd and S precursors, respectively. As shown in Fig. S2,† a dense layer of CdS is formed on the surface of each Fe_3O_4/RGO nanosheet, which is built up of thousands of small CdS crystals. It can be seen from the HRTEM images in Fig. S2† that the lattice spacing of 0.33 nm corresponds well with the characteristic (111) planes of hexagonal CdS. An EDX analysis has also been undertaken, with the data shown in Fig. S3,† and the results have firmly confirmed the presence of Fe, Cd and S elements in the final products.

Finally, the deposition of Au NPs was accomplished by using sodium citrate (Na_3Cit) to reduce $HAuCl_4$ in a boiling aqueous solution. The corresponding TEM images are shown in Fig. 1, and it is easy to distinguish the formation of the ultra-small Au NPs on CdS's surface *via* their deeper contrast (Fig. 1B and C). The loading amount of Au could be controlled well by directly changing the $HAuCl_4$ feed amount. The samples with different Au amounts are named as Au/CdS/Fe_3O_4/RGO-1 (Au: 1 wt%), Au/CdS/Fe_3O_4-2 (Au: 3 wt%), and Au/CdS/Fe_3O_4-3 (Au: 5 wt%).

The evolution process of the products could also be seen from the powder X-ray diffraction (XRD) patterns. The data of the synthesized pure CdS, Fe_3O_4/RGO, CdS/Fe_3O_4/RGO and Au/CdS/Fe_3O_4/RGO-1 nanocomposites are shown in Fig. S4.† Compared with the characteristic diffraction peak at 2θ = 10.6° in the XRD pattern of disordered GO, the absence of this peak in the XRD patterns of as-obtained Fe_3O_4/RGO, CdS/Fe_3O_4/RGO and Au/CdS/Fe_3O_4/RGO nanocomposites indicates the conversion of GO to RGO. The other diffraction peaks in the XRD patterns of the nanocomposites can be indexed to the magnetite Fe_3O_4 (JCPDS card no. 19-0629) or hexagonal CdS (JCPDS no. 65-3414): six representative diffraction lines are observed in the XRD pattern of Fe_3O_4 at 2θ = 30.2°, 35.6°, 43.3°, 53.7°, 57.3°, and 62.8°. These diffraction lines can be assigned to the (220), (311), (400), (422), (511) and (440) reflections, respectively, of the pure cubic spinel crystal structure of Fe_3O_4 with the cell constant a = 8.39 Å. The other six strong diffraction peaks at 2θ = 24.9°, 26.5°, 28.2°, 43.8°, 47.8° and 51.9° can be assigned to the (100), (002), (101), (110), (103) and (112) crystal planes of the hexagonal CdS. Unfortunately, no evident diffraction signal of Au NPs was detected, which may be caused by their smaller particle size, poor crystallinity and low content compared with Fe_3O_4 and CdS.

Fig. S5† shows the survey XPS spectra of the Au/CdS/Fe_3O_4/RGO composites. After the synthetic reaction, the peak

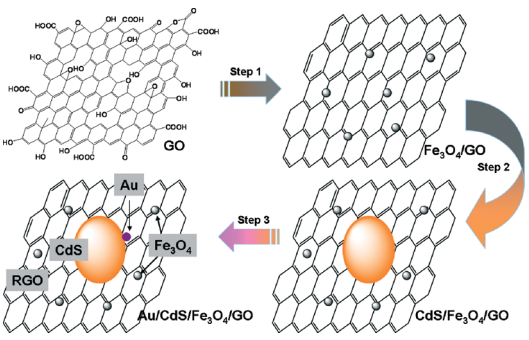

Scheme 1 Schematic diagram for the formation of Au/CdS/Fe_3O_4/RGO nanocomposites.

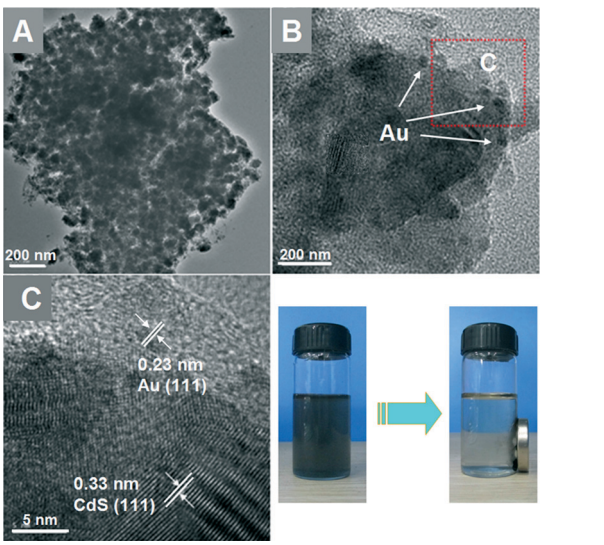

Fig. 1 TEM images of Au/CdS/Fe_3O_4/RGO-1 (A) to (C); and photographs of the sample dispersed in aqueous solution (left) without and (right) with an external magnetic field.

associated with C=C–C (284.6 eV) became predominant, while the peaks related to the oxidized carbon species, such as C–OH (285.2 eV), C–O (286.7 eV) and O–C=O (288.4 eV) were greatly weakened. These results indicate that GO has been deoxygenated well to form graphene, which is very important for improving its conductivity and the stability of the composites. The binding energies of Cd $3d_{5/2}$ were found at 404.8–404.9 eV for CdS, suggesting that cadmium was in the Cd^{2+} state. The S $2p_{3/2}$ peaks were observed at 161.9–162.0 eV, in agreement with the expectation that sulphide existed as S^{2-}.

Fig. 2A shows the profile of the photocatalytic degradation efficiency of Methylene Green (MG) catalyzed by pure CdS, CdS/Fe_3O_4/RGO and the Au/CdS/Fe_3O_4/RGO nanocomposites under VL irradiation ($\lambda > 420$ nm). Adsorption for a period of time in the dark was essential to reach equilibrium before timing. After 30 min irradiation, the degradation degree of MG for the Au/CdS/Fe_3O_4/RGO-1 nanocomposites attained almost 100%, which was the highest catalytic activity among the five as-obtained catalysts. For pure CdS NPs, their catalytic capabilities are very limited. They could convert only about 30% MB, even after irradiation for 60 min, while the CdS/Fe_3O_4/RGO nanocomposites had a better catalytic activity, but still much lower than that of Au/CdS/Fe_3O_4/RGO-1. The mechanism of the enhancement of the photocatalytic activity of CdS by the introduction of RGO and Au is suggested as follows. Under VL irradiation, electrons are excited from the valence band (VB) to the conduction band (CB) of the CdS semiconductor, leaving positive charged holes in the VB. Without RGO, electrons will transit from the CB to the VB, owing to the instability of the excited states, resulting in a significantly lower catalytic activity with the dyes. Once RGO is introduced, it plays the role of electron acceptor and transporter to efficiently hinder the recombination of the photogenerated electron–hole pairs, leaving more charge carriers to form reactive species. Meanwhile, dye molecules tend to be accumulated on the surface of the catalysts because of the strong π–π conjugation between the RGO and dyes. The 1 wt% amount of Au NPs also intensifies the catalytic activity further.

For further comparison, Fig. 2B shows the photodegradation efficiency of MG and some other dyes (Acid Fuchsin, Eosin B and Rhodamine B (RhB)) for the Au/CdS/Fe_3O_4/RGO-1 nanocomposite under VL irradiation. After 60 min irradiation, the amounts of unconverted dye are around 67%, 48% and 7% for Acid Fuchsin, Eosin B and RhB, respectively. The totally different catalytic performance might be the result of the following parameters. Dyes are first dissolved in water and in the form of ions. As we know, the surface charge of RGO is negative, which makes the RGO surface more conducive to adsorbing the dye ions with positive charges, so that the Au/CdS/Fe_3O_4/RGO sample has a higher catalytic activity towards alkaline dyes than acidic dyes. In addition, a cycling test of the Au/CdS/Fe_3O_4/RGO-1 sample has been done. As shown in Fig. S10,† after 5 successful cycles, Au/CdS/Fe_3O_4/RGO-1 also exhibited very high photocatalytic activity. After 30 min irradiation, over 90% MG has been degraded. This result has firmly confirmed that this hybrid nanostructure is highly stable.

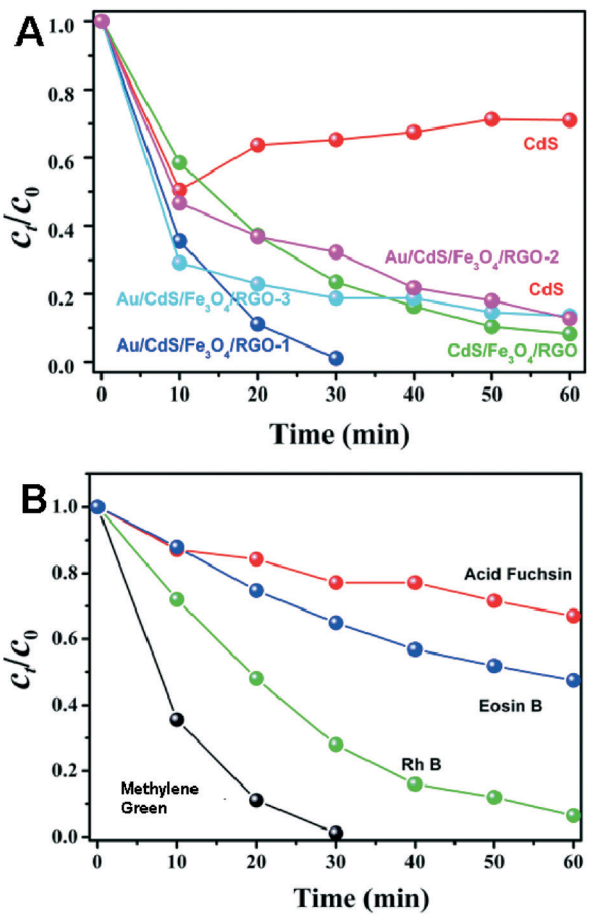

Fig. 2 (A): Photocatalytic degradation of MG by CdS, CdS/Fe_3O_4/RGO, Au/CdS/Fe_3O_4/RGO-1, Au/CdS/Fe_3O_4/RGO-2 and Au/CdS/Fe_3O_4/RGO-3; (B): Photocatalytic degradation of MG, RhB, Eosin B and Acid Fuchsin by Au/CdS/Fe_3O_4/RGO-1.

Conclusions

In conclusion, we have successfully developed a new facile multi-step method to hybridize multiple components, including GO, Fe_3O_4, CdS and Au, together to form a single entity. Therein, Fe_3O_4 provides the magnetic properties, CdS is the active center with high photocatalytic activity and Au plays the role of co-catalyst. More importantly, the RGO nanosheets are indispensable. They act not only as a supporter to hold the multiple components together, but also as an electron acceptor and transporter to efficiently hinder the recombination of the photo-generated electron–hole pairs. It is believed that such a magnetic nanocatalyst could have great application prospects in the field of environmental technology and the layer-by-layer synthetic process may have great significance in guiding the design and preparation of highly efficient multi-functional nanomaterials.

Acknowledgements

This work was supported by the Program for the Fund Project of Science and Technology of Education Department of Jilin Province (2014056) and the Science Foundation of Jilin Province (20110904).

References

1 T. Y. Peng, K. Li, P. Zeng, Q. G. Zhang and X. G. Zhang, *J. Phys. Chem. C*, 2012, **116**, 22720.
2 X. W. Wang, H. W. Tian, Y. Yang, H. Wang, S. M. Wang, W. T. Zheng and Y. C. Liu, *J. Alloys Compd.*, 2012, **524**, 5.
3 H. Fujiwara, H. Hosokawa, K. Murakosi, Y. Wada and S. Yanagida, *J. Phys. Chem. B*, 1997, **101**, 8270.
4 Q. Li, B. D. Guo, J. G. Yu, J. R. Ran, B. H. Zhang, H. J. Yan and J. R. Gong, *J. Am. Chem. Soc.*, 2011, **133**, 10878.
5 L. Sheeney-Haj-Ichia, B. Basnar and I. Willner, *Angew. Chem., Int. Ed.*, 2005, **44**, 78.
6 H. Park, W. Choi and M. R. Hoffmann, *J. Mater. Chem.*, 2008, **18**, 2379.
7 X. W. Wang, G. Liu, Z. G. Chen, F. Li, L. Z. Wang, G. Q. Lu and H. M. Cheng, *Chem. Commun.*, 2009, 3452.
8 X. Zong, H. J. Yan, G. P. Wu, G. J. Ma, F. Y. Wen, L. Wang and C. Li, *J. Am. Chem. Soc.*, 2008, **130**, 7176.
9 H. J. Yan, J. H. Yang, G. J. Ma, G. P. Wu, X. Zong, Z. B. Lei, J. Y. Shi and C. Li, *J. Catal.*, 2009, **266**, 165.
10 H. N. Kim, T. W. Kim, I. Y. Kim and S. J. Hwang, *Adv. Funct. Mater.*, 2011, **21**, 3111.
11 R. M. Navarro, F. del Valle and J. L. G. Fierro, *Int. J. Hydrogen Energy*, 2008, **33**, 4265.
12 K. S. Novoselov, A. K. Geim, S. V. Morozov, D. Jiang, Y. Zhang, S. V. Dubonos, I. V. Grigorieva and A. A. Firsov, *Science*, 2004, **306**, 666.
13 A. K. Geim and K. S. Novoselov, *Nat. Mater.*, 2007, **6**, 183.
14 P. Gao, J. C. Liu, S. Lee, T. Zhang and D. D. Sun, *J. Mater. Chem.*, 2012, **22**, 2292.
15 N. Zhang, Y. H. Zhang, X. Y. Pan, X. Z. Fu, S. Q. Liu and Y. J. Xu, *J. Phys. Chem. C*, 2011, **115**, 23501.
16 J. L. Wu, S. Bai, X. P. Shen and L. Jiang, *Appl. Surf. Sci.*, 2010, **257**, 747.
17 C. F. Zhou, Z. H. Wang, J. F. Xia, B. K. Via, F. F. Zhang, Y. Z. Xia and Y. H. Li, *C. R. Chim.*, 2012, **15**, 714.
18 T. Zeng, X. L. Zhang, Y. R. Ma, H. Y. Niu and Y. Q. Cai, *J. Mater. Chem.*, 2012, **22**, 18658.
19 X. Y. Li, X. Wang, S. Y. Song, D. P. Liu and H. J. Zhang, *Chem. – Eur. J.*, 2012, **18**, 7601.
20 X. Y. Yang, X. Y. Zhang, Y. F. Ma, Y. Huang, Y. S. Wang and Y. S. Chen, *J. Mater. Chem.*, 2009, **19**, 2.

